Identification of Noise Sources by Means of Inverse Finite Element Method

M. Weber[*,1], T. Kletschkowski[2] and B. Samtleben[3]
[1,2]Helmut-Schmidt-University Hamburg, [3]Airbus Germany
*Corresponding author: Holstenhofweg 85, 22043 Hamburg, Germany. Email: mweber@hsu-hh.de

Abstract: An inverse finite element method for noise source identification in an aircraft cabin is presented. If all sound sources are located on the boundary on the cabin, the equation system resulting from a matching FE model can be re-sorted in such a way that computation of the unknown boundary data is possible from measurement data taken in the cavity.
The method is first validated using a simplified 3D COMSOL model. The numerically calculated data inside an inner sub-domain are impinged with a stochastic error and used as simulated measurement data to re-calculate the boundary data.
In a next step, the sound field in the cavity of an aircraft mock-up excited by both interior and exterior noise sources is mapped with a custom-built microphone array. A matching COMSOL model is verified and compared to the mapping data. Consequently the inverse calculation is performed for this more realistic model.

Keywords: FE model, acoustics, inverse methods, noise source identification.

1. Introduction

Aircraft cabin noise is a key factor for the perception of cabin comfort of passengers in civil aircraft. Improvements in cabin noise are hard to reach with the constraints: no additional weight, approved materials only, no impact on visual appearance of cabin parts, and industrial design.

However, reduction of cabin noise levels together with a reduction of aircraft fuselage and cabin lining weight requires precise information about the localization and quantification of the dominant noise sources. Reducing the impact of the major sources is the “cheapest” way to reduce cabin noise significantly (or to cope with the consequences of weight reduction measures). This leads to the need of a measurement tool which is able to localize and quantify noise sources which are in fact weaknesses of the insulating capability of cabin lining or locally increased noise loads.

Usual methods for noise source localization from simple sound pressure or intensity measurements to 2D “acoustic cameras” by beamforming [1,2] or near field holography [3,4,5,6] have all specific drawbacks. E.g., beamforming methods cannot distinguish between reflected or radiated waves. Since the noise in an aircraft cabin is radiated from all parts of the cabin lining in almost every direction, strong reflections can occur on a part that itself radiates only low noise.

A method that uses information of the pressure distribution in a relatively small control volume to calculate position and power of sources on the cabin boundary promises an effective and fast possibility to analyze an aircraft cabin during flight.

The inverse finite element method (IFEM) presented in this paper reconstructs the distribution of sound pressure and particle velocity in the interior of the cabin based on a standard FE model, see [7,8,9,10]. From a certain subspace of the interior, referred to as measurement area, data are taken and used as boundary conditions for the IFEM that will predict the sound field in the complete area, including the boundaries between interior and structure. Examining sound pressure and particle velocity on these boundaries, conclusions can be drawn to the location of acoustic hot spots.

2. Noise Source Identification by inverse FEM

The FE method for the time-harmonic analysis of weakly damped interior noise problems is based on the Helmholtz equation

$$\Delta p(\mathbf{x}) + k^2 p(\mathbf{x}) = 0, \qquad (1)$$

where Δ represents the Laplace operator and $k = 2\pi f / c$ the wave number that is determined by the excitation frequency f and the speed of sound

c. The corresponding boundary conditions (BC) are given by the Dirichlet BC for the acoustic pressure

$$p = \overline{p} \quad \text{on } R_p, \tag{2}$$

and the Neumann BC for the normal component of particle velocity

$$-\mathbf{n}\cdot\frac{1}{\rho}\nabla p = i\left(2\pi f\right)\overline{v}_n \quad \text{on } R_v. \tag{3}$$

Discretization of Eq. (1) using the FE method leads to a set of algebraic equations for the sound pressure that can be summarized as

$$\mathbf{K}\mathbf{p} = \mathbf{v}. \tag{4}$$

K is the stiffness matrix, **p** the vector of the excess pressure and **v** a vector that is proportional to the particle velocity in the sound field, and therefore called generalized velocity vector. The solution of Eq. (4) with respect to the BC leads to the unknown pressure field **p**. This process is called forward calculation.

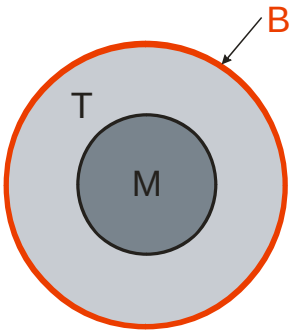

Fig. 1: Spatial domain decomposition

In order to derive the IFEM the calculation domain is split into three regions: an inner measurement sub-domain (M), a transition sub-domain (T), and an outer boundary (B) as illustrated in Fig. 1. It is possible to decompose Eq. (4) as follows:

$$\begin{bmatrix}\mathbf{K}_1 & \mathbf{K}_2 & \mathbf{K}_3\\ \mathbf{K}_4 & \mathbf{K}_5 & \mathbf{K}_6\\ \mathbf{K}_7 & \mathbf{K}_8 & \mathbf{K}_9\end{bmatrix}\begin{bmatrix}\mathbf{p}_{MK}\\ \mathbf{p}_{TU}\\ \mathbf{p}_{BU}\end{bmatrix} = \begin{bmatrix}\mathbf{v}_{MK}\\ \mathbf{v}_{TK}\\ \mathbf{v}_{BU}\end{bmatrix}. \tag{5}$$

The first index of the three sound pressure sub-matrices $\mathbf{p}_{ij}$ and the three sub-matrices $\mathbf{v}_{ij}$ of the generalized velocity vector **v** denotes the sub-domain of the decomposed calculation domain, whereas the second index denotes whether the variable is known (K) or unknown (U).

As described in [9], in the absence of unknown volume sources in the transition and measurement sub-domain the unknown parts of the sound pressure vector **p** can be computed by the solution of a reduced problem that is given by

$$\begin{bmatrix}\mathbf{K}_2 & \mathbf{K}_3\\ \mathbf{K}_5 & \mathbf{K}_6\end{bmatrix}\begin{bmatrix}\mathbf{p}_{TU}\\ \mathbf{p}_{BU}\end{bmatrix} = \begin{bmatrix}-\mathbf{K}_1\mathbf{p}_{MK}\\ -\mathbf{K}_4\mathbf{p}_{MK}\end{bmatrix}. \tag{6}$$

$$\begin{bmatrix}\mathbf{K}_8 & \mathbf{K}_9 & -\mathbf{I}\end{bmatrix}\begin{bmatrix}\mathbf{p}_{TU}\\ \mathbf{p}_{BU}\\ \mathbf{v}_{BU}\end{bmatrix} = \begin{bmatrix}-\mathbf{K}_7\mathbf{p}_{MK}\end{bmatrix} \tag{7}$$

leads to the unknown velocities at the outer boundary. This procedure is called inverse calculation.

Eq. (6) can be solved to determine the complete sound field in the interior using only the measurements in the inner region of the sound field. For simplicity it is rewritten as follows:

$$\mathbf{A}\mathbf{x} = \mathbf{b}; \tag{8}$$

$$\mathbf{A} \equiv \begin{bmatrix}\mathbf{K}_2 & \mathbf{K}_3\\ \mathbf{K}_5 & \mathbf{K}_6\end{bmatrix}, \mathbf{x} \equiv \begin{bmatrix}\mathbf{p}_{TU}\\ \mathbf{p}_{BU}\end{bmatrix}, \mathbf{b} \equiv \begin{bmatrix}-\mathbf{K}_1\mathbf{p}_{MK}\\ -\mathbf{K}_4\mathbf{p}_{MK}\end{bmatrix}.$$

As stated in [7] it has been found that the condition number of the new portioned stiffness matrix **A** is very high, especially if realistic measurement errors are taken into account. Therefore, several regularization techniques such as Truncated Singular Value Decomposition (TSVD), Tikhonov Regularization (TR) or Conjugated Gradient Least Squares (CGLS) have been applied to solve the ill-posed problem that is given by Eq. (8).

More details about the regularization algorithms that have been used to solve Eq. (8) can be found in previous publications. The implementation of the TSVD and TR is described in [7, 8, 9].

3. Realization with MATLAB and COMSOL

The implementation of the IFEM method was done in MATLAB, using COMSOL commands to extract the required data. First, a COMSOL geometry model was built (Helmholtz Equation PDE mode, linear Lagrange elements) and an inner sub-domain defined. For simulation, a noise source was added (by applying a normal acceleration boundary condition). The following information is required to perform the IFEM:

- the stiffness matrix **K**,
- the sound pressure values corresponding to the mesh points belonging to the inner sub-domain, and thus
- the indices of the mesh points belonging to either inner sub-domain, outer sub-domain or boundary.

For application with measured data, the excitation frequency has to be written into the 'fem' struct to extract the stiffness matrix. Also, a preprocessing step is required to interpolate the mapped data to the mesh points. For both measured and simulated data, no *a priori* information on the boundary conditions is necessary – on the contrary, the boundary impedance can be deduced from the results of the IFEM.

4. Validation Using Simplified 3D Simulation

In two dimensions, the IFEM had already been validated for both simulated [9] and measured data [10]. Three-dimensional validation was first performed with a simple box model containing a normal acceleration source in the boundary. The mesh consisted of 3316 points, 1101 of which were located on the boundary. The inner sub-domain was chosen in such a way that it contained 1431 points. As can be derived from the resorted matrix **A** in Eq. (7), this means that the resulting problem is over-determined.

Fig. 2a shows the COMSOL simulation, excited with f = 400Hz. The boundary conditions were set rigid here. The sound pressure values inside the inner sub-domain were then impinged with a stochastic error of up to 5 percent to simulate noisy measurement data. The result of the inverse calculation based on these data is shown in Fig. 2b. As a regularization technique, TSVD was used; the optimal regularization parameter was estimated by L-Curve analysis [11]. The sound field in the outer sub-domain, and thus, the location of the source was clearly reconstructed.

a)

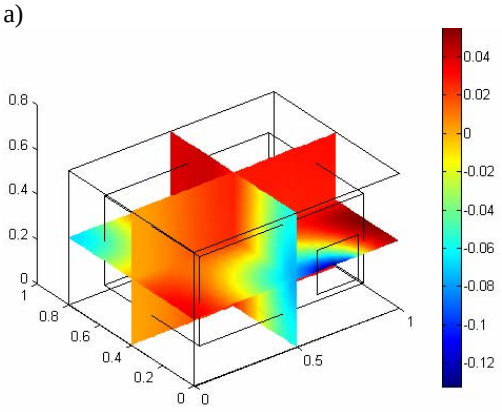

b)

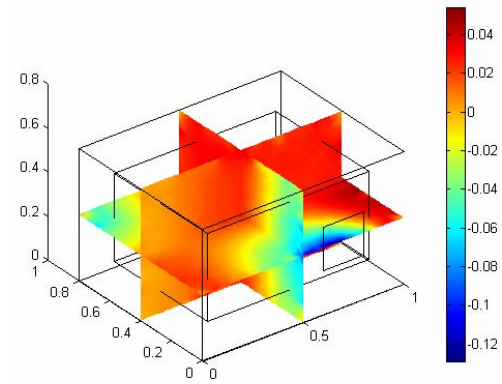

Fig. 2: Simulated (a) and reconstructed (b) sound pressure field, linear scale

5. Application in an Aircraft Mock-up

5.1. Mapping of the Mock-up

In the next validation step, the sound field inside a special acoustic mock-up for a long range aircraft cabin has been measured. 7172 microphone positions with a 170 mm spacing in a regular grid have been used to determine transfer functions between a loudspeaker in one corner of the fuselage section and the respective

microphone. A second set of data was measured with loudspeakers outside the mock-up and in a position and distance which is typical to jet noise excitation. All measurement microphones were placed on a rig covering the whole cross section, which was torn along the cabin mock-up.

Fig. 3 shows the interior of the mock-up with the built-in measuring apparatus; the dimensions of the mock-up and the measurement grid are illustrated in Fig. 4.

Fig. 3: Measuring apparatus inside the mock-up

a)

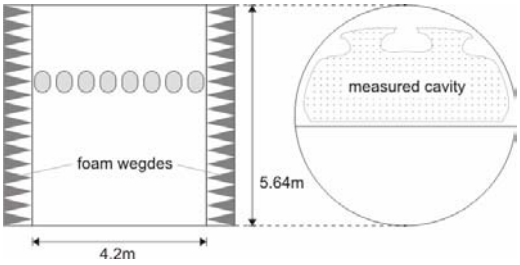

b)

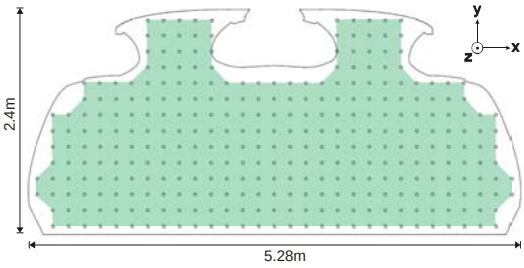

Fig. 4: Dimensions of the mock-up (a) and the measured cavity (b) including measuring grid

The transfer functions were measured in magnitude and phase with wideband noise excitation.

5.2. Validation of the FE Model

In order to verify the corresponding FE model of the cavity as shown in Fig. 5, its convergence had to be secured. For this purpose, all boundaries were defined to be sound-hard. Ten eigenfrequencies around 200Hz were numerically calculated for different meshes with a growing number of DOF. This was achieved by relating the maximum element size to the wavelength λ, correlating to a maximum frequency of $f_{\max}$ = 300Hz:

$$d_{\max} = \lambda / n; \quad \lambda = c / f_{\max}; \quad n = 4,5,...,11. \quad (9)$$

Fig. 5: FE model of the cavity

Since the distance between the single eigenfrequencies had the same order of magnitude as the amount each eigenfrequency decreased with every step of refinement, the matching eigenfrequencies were identified using the Modal Assurance Criterion (MAC)

$$\frac{\left|\{\psi_A\}^H \{\psi_B\}\right|^2}{\{\psi_A\}^H \{\psi_A\} \{\psi_B\}^H \{\psi_B\}}. \quad (10)$$

The MAC is a scalar constant rating the causal relationship between two modal vectors $\{\psi_A\}$ and $\{\psi_B\}$. It takes on values between zero, implying no consistent correspondence, to one, signifying a consistent correspondence [12]. By means of the MAC, the variances of eight

eigenfrequencies could be monitored with growing mesh refinement. In Fig. 6, the number of DOF is plotted against the variance of each eigenfrequency from one refinement step to another. For the step from 69266 DOF to 92084 DOF, the variance is less than 0.1 %, so 69266 DOF corresponding to $d_{max} = \lambda/9$ is considered sufficient.

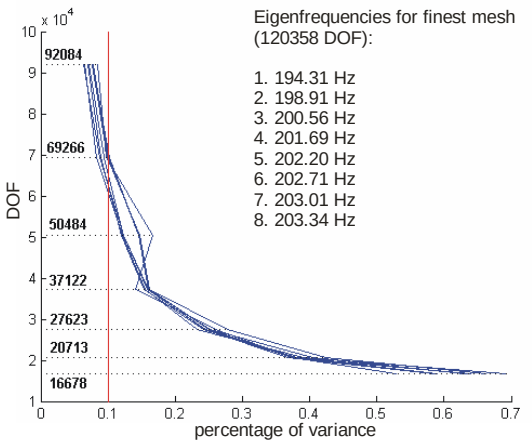

Fig. 6: Convergence of the FE model

Comparison of Model and Mapping

In the mock-up, the ends of the fuselage are not sound-hard but closed with absorbing material. As stated in chapter 3, for the application of the IFEM no knowledge about the boundaries in required (in fact, a near free field impedance resulting for the fuselage ends may be another factor for the validation of the IFEM). Nevertheless, to perform a forward calculation that roughly estimates the sound field excited by the internal loudspeaker, the ends were given a free field impedance BC. A normal acceleration BC was applied at the location of the loudspeaker, and the remaining boundaries were left sound-hard.

Fig. 7 illustrates a slice plot of the symmetry plane of the fuselage referring to the two absorbing ends, of the numerical result for f = 293Hz and the corresponding plots for internal and external loudspeaker excitation. This frequency was chosen because it showed a significant peak on a number of frequency response plots of the measured data.

a) numerical result (f = 293Hz)

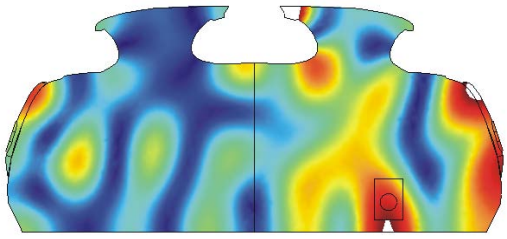

b) measured data (f = 293Hz, internal loudspeaker)

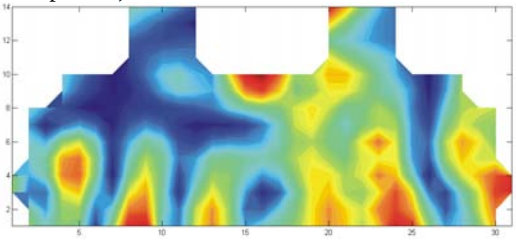

c) measured data (f = 293Hz, external loudspeaker)

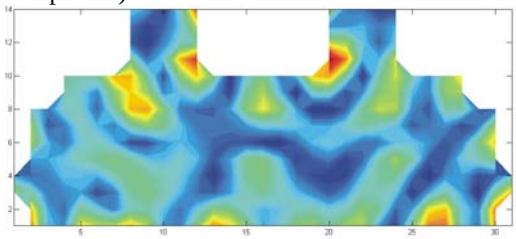

Fig. 7: Slice plots for numerical result (a) and measured data with internal (b) and external (c) loudspeaker. (a) contains the projection of the speaker's position. Shown is the magnitude of the sound pressure in linear scale.

The amplitude values are not significant in these plots; the scale was adapted to enable merely a qualitative comparison. Despite the rough estimation of the BC, there are obvious similarities between the numerical result and the measured data for internal excitation. For excitation with the external speaker, however, the distribution of sound pressure differs significantly.

5.3. Inverse Calculation using Mock-up Model and Measured Data

With the now validated model, the inverse calculation performed in chapter 4 was repeated, using the measurement data with the loudspeaker located inside the cabin. Because the pressure values were complex now, preliminarily a coarser mesh was used to reduce computing time. To keep up the accuracy, a lower frequency (f = 90Hz) was chosen. An inner sub-domain was defined as shown in Fig. 8.

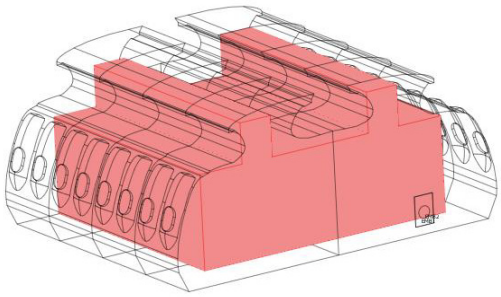

Fig. 8: Cavity model with inner sub-domain

The mesh now consisted of 27047 points, 8678 of which were located on the boundary and 9895 in the inner sub-domain. The pressure values measured at positions located inside the inner sub-domain were linearly interpolated to the mesh points. Fig. 9a shows the magnitude of the interpolated data (cross section plot of the symmetry plane of the fuselage), Fig. 9b and 9c show the result of the inverse calculation using CGLS and Tikhonov regularization, both with NCP parameter choice method [13]. The CGLS solution seems slightly over-regularized, as the pressure values decrease while approaching the rigid boundary. The Tikhonov solution on the other hand has some oscillations at the boundary that are typical for under-regularized ill-posed problems.

However, the CGLS method delivers the best solution if we consider the normal velocity, which is proportional to the pressure gradient, on the boundary. Fig. 10 shows the boundary plane that, as we know, contains the sound source. The location of the source is nearly exactly reconstructed.

a) interpolated values from measurement

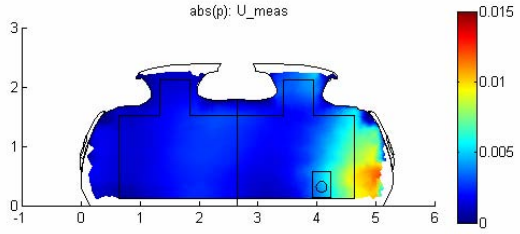

b) inverse calculation, CGLS

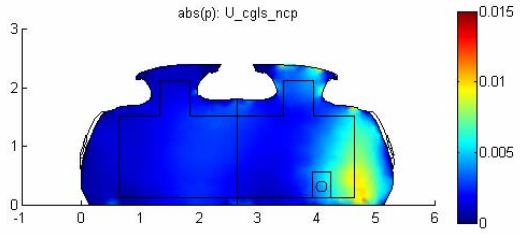

c) inverse calculation, Tikhonov

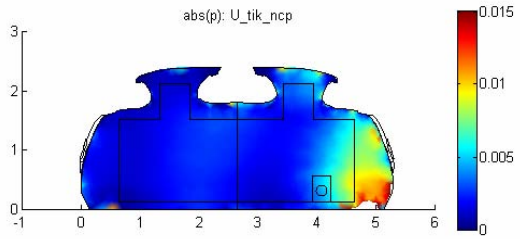

Fig. 9: Magnitude of sound pressure from measurement and inverse calculation (cross-section plot, linear scale)

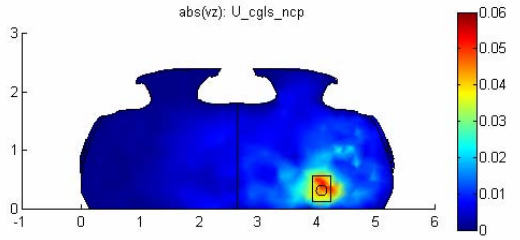

Fig. 10: Norm of pressure gradient on “front” boundary plane showing position of loudspeaker

6. Summary and Outlook

In the first part of this paper, an inverse finite element method for noise source identification was presented. In order to verify the IFEM, a simulation was successfully applied using a simple three-dimensional geometry. In the second part, the IFEM was applied in more real-life conditions, with measured data taken from an aircraft mock-up. By means of a matching FE model, the location of a sound source placed on the boundary of the mock-up could be identified.

In upcoming research, the IFEM technique will have to be stabilized and made numerically more efficient, sensitivity studies concerning the reduction of measurement data will be performed to make the method more applicable, and the calculation will be repeated using the data measured with external loudspeaker excitation.

Acknowledgments

The authors would like to thank Mr. Kai Simanowski, Mr. Oliver Pabst (Helmut-Schmidt-University) as well as Mr. Dirk Henny (Airbus) for their support during the mapping of the mock-up.

References

[1] J. Christensen, J. Hald, “Beamforming”, Technical Review, Brüel & Kjaer, No. 1 (2004)

[2] K. R. Holland, P. A. Nelson, “Sound source characterisation: The focused beamformer vs the inverse method”, 10th Int. Congress on Sound and Vibration, Stockholm (2003)

[3] J. Hald, “Non-stationary STSF”, Technical Review, Brüel & Kjaer, No. 1 (2000)

[4] J. D. Maynard, E.G. Williams, Y. Lee, “Nearfield acoustic holography: Theory of generalized holography and the development of NAH”, J. Acoust. Soc. Am. 78(4), 1395-1413 (1985)

[5] R. Reibold, “Sound source reconstruction using fourier optics”, Acustica 63, 60-64 (1987)

[6] E. G. Williams, “Fourier Acoustics”, Academic Press, London (1999)

[7] J. Drenckhan, D. Sachau, “Identification of sound sources using inverse FEM”, Proceedings of the 11th Int. Congress on Sound and Vibration, Stockholm (2003)

[8] J. Drenckhan, D. Sachau, “Identification of sound sources using inverse FEM”, 7th Int. Symposium “Transport Noise and Vibration“, St. Petersburg (2004)

[9] D. Sachau, J. Drenckhan, T. Kletschkowski, S. Petersen, “Entwicklung von Mess-techniken zur Lärmquellenidentifizierung in Kabinen“, Final report LUFO HH TUT-34, Helmut Schmidt University/ University of the Federal Armed Forces Hamburg (2005)

[10] M. Weber, T. Kletschkowski, D. Sachau, “Identification of noise sources by means of inverse finite element method using measured data”, Acoustics’08, Paris

[11] P. C. Hansen, “Rank-Deficient and Discrete Ill-Posed Problems”, Vol. 1, Society for Industrial and Applied Mathematics, Philadelphia (1998)

[12] R. J. Allemang, D. L. Brown, “A Correlation Coefficient for Modal Vector Analysis”, Proceedings, Int. Modal Analysis Conference, 110-116 (1982)

[13] P. C. Hansen, M. E. Kilmer, R. H. Kjeldsen,“Exploiting Residual Information in the Parameter Choice for Discrete Ill-Posed Problems“, BIT Numerical Mathematics (2006) 46: 41-59, Springer